



# Numerical model of inclusion separation from liquid metal with consideration of dissolution in slag

Wei Liu<sup>1</sup> · Shu-feng Yang<sup>1</sup> · Jing-she Li<sup>1</sup> · Feng Wang<sup>1</sup> · Hong-bo Yang<sup>2</sup>

Received: 26 July 2018 / Revised: 10 December 2018 / Accepted: 11 December 2018 / Published online: 1 January 2019  
© China Iron and Steel Research Institute Group 2019

## Abstract

The transport of inclusion particles through the liquid metal/molten slag interface and their dissolution in the slag are two key processes of inclusion removal. Based on the latest version of inclusion transport model that takes into account full Reynolds number range and a dissolution kinetics model, a coupled model was developed to simulate the whole process of inclusion removal, from floating in the liquid steel to crossing the interface and further to entering and dissolving in the molten slag. The interaction between the inclusion motion and dissolution was discussed. Even though the inclusion velocity is a key parameter for dissolution, the simulation results show no obvious dissolution during moving state because the process is too short and most of the inclusions dissolve during its static stay in the slag side above the interface. The rate-controlling step of inclusion removal is the transport through the steel–slag interface for the small-size inclusion and static dissolution above the interface for the large-size inclusion, respectively.

**Keywords** Inclusion removal · Slag dissolution · Inclusion separation · Clean steel · Secondary refining

## 1 Introduction

A key to improve metal product quality is to obtain high cleanliness, that is, to remove inclusions as many as possible [1, 2]. Inclusions are usually nonmetallic particles trapped in the metal matrix, which will break the continuity of metal and thus degrade the mechanical performance [3]. Although there have been several novel methods of inclusion removal, such as electromagnetic [4] and super-gravity [5] field, the main way is still slag absorption [6, 7]. The inclusion removal by slag absorption has three steps: (1) nucleation, growth and floatation of inclusions in the liquid metal; (2) contacting with the metal/slag interface and entering the slag phase; and (3) dissolving in the molten slag and finally disappearing. Each of the three

steps has been separately studied both in experimental and numerical ways [8–15].

The inclusion dissolution process, with the help of high-temperature confocal laser scanning microscopy (CLSM) [16], has obtained a comprehensive kinetics model for dissolution [13, 17–20]. As for the inclusion transport through the interface, the process is related to complex fast-changing dynamic forces including buoyancy, drag force, interface tension and added mass force, which is not easy to describe. Nakajima and Okamura [21] built a model to simulate the inclusion motion at the interface based on force balance. The model was then used to examine solid [22] and liquid [23] nonmetallic inclusions at different interfaces with various properties. By applying the inclusion at the metal/slag interface model, the critical condition for inclusion crossing the interface could be obtained. Liu et al. [24, 25] developed a model by expanding the Reynolds number ( $Re$ ) range of inclusions (from  $0 < Re < 1$  to  $Re > 1$ ), which guarantees more accuracy of the drag force of inclusions. Besides, the model is more adaptive to various conditions of interface crossing, and the model validation is realized by comparing the results of numerical

✉ Shu-feng Yang  
yangshufeng@ustb.edu.cn

<sup>1</sup> School of Metallurgical and Ecological Engineering,  
University of Science and Technology Beijing,  
Beijing 100083, China

<sup>2</sup> National Engineering Research Center for Rare Earth  
Materials, General Research Institute for Nonferrous Metals,  
Beijing 100088, China

simulation with water model experiment. Even more, with this developed model, the calculation of floating terminal velocity of inclusions in steel is more realistic at high  $Re$ , and the floating terminal velocity, which is also the contact velocity of inclusions with the interface, defines the initial momentum of the inclusion at the interface.

The chemical reactions of inclusions with slag are always ignored in the models of inclusion motion, which is based on the assumption that the crossing interface time is so short and no obvious dissolution of inclusion will occur during this process. However, Yan et al. [16] pointed out that motion and rotation of inclusions will speed up the dissolution rate in the slag phase. Thus, during the moving at the interface and in the slag, whether the inclusion dissolution can be neglected remains unclear. What is more, the inclusion size in the motion model is a quite important parameter, which determines the forces and thus changes the acceleration of inclusions. If there is a small change in the size, the position and state of inclusion will be affected greatly. Therefore, a model of inclusion motion in fluids with consideration of dissolution reaction should be built to evaluate the interaction effects with each other. Shannon and Sridhar [26] first calculated the dissolution time of 1.5- and 10- $\mu\text{m}$  inclusions separating at the steel–slag interface, and the results showed that during the separation time of inclusions, no apparent dissolution happened.

Based on the latest version of inclusions at interface (IAT) model [11, 24, 25] that adapts full  $Re$  range of inclusions and the CLSM observation validated dissolution kinetics model [11, 24, 25] which considers the moving state of inclusions, a combination model that simulates the whole process of inclusion removing, from floating in the liquid steel to crossing the interface and further to entering the molten slag, has been built and the influences between the processes have been discussed. The questions that what kind of inclusions can pass the interface and enter the slag phase and how they move, dissolve and finally are removed in the slag will be answered.

## 2 Modeling

The influence considering inclusion dissolution should be evaluated in the model because the process of dissolution will result in size change of inclusions. The initial radius of inclusions is used as a fixed value for the calculation of the dimensionless displacement in this model. The other calculating equations containing inclusion radius or size, i.e., the  $Re$  number of inclusions, are using the dynamic values. A lot of other details should be modified to consider the dissolution in the motion model of inclusions.

### 2.1 Assumptions

1. The change of slag properties due to inclusion dissolution or temperature change is neglected.
2. The dissolution at the surface of an inclusion is uniform, and the inclusion keeps spherical in shape.
3. The inclusion floats and contacts the interface with its floating terminal velocity in the steel.
4. The slag phase is thick enough so that the condition of inclusion floating to the slag surface is not in consideration.
5. The rotation of inclusions is not considered in this model.

### 2.2 Model of inclusion motion at interface

The motion model of inclusions near and at the interface is based on the force balance, and the latest version with more details can be found in previous studies [11, 24, 25]. In this study, a solid spherical  $\text{Al}_2\text{O}_3$  inclusion moving in liquid steel and a typical refining slag are simulated. During the process of moving, the drag force, buoyancy, gravity, added mass force and interface tension are considered. The properties of the interface, like viscosity and density, should be considered as a mixture of the two liquids and related to the relative position to the interface of inclusions. It should be pointed out that, since the  $Re$  range in the model covers both the real motion of inclusions at steel–slag interface and the motion in the water model, the numerical model is considered to be validated if the numerical motion model simulates the condition of water model experiment with a hollow  $\text{Al}_2\text{O}_3$  sphere moving at water and silicone oil interface well [11].

### 2.3 Inclusion dissolution model

When the inclusion is moving at the interface or in the slag phase, the velocity relative to the surrounding fluid makes the concentration outside the boundary to be renewed continuously. Yan et al. [16] evaluated the dissolution mechanism of  $\text{MgO}$  and  $\text{Al}_2\text{O}_3$  in metallurgical slag based on the literature data of CLSM experimental results. The effect of fluid flow around the inclusion was taken into account to calculate the mass transfer rate. The dissolution mass of inclusions is given by:

$$dM_p = \rho_p dV = \rho_p 4\pi R^2 dR \quad (1)$$

where  $M_p$  is the mass of inclusion particle, kg;  $\rho_p$  is the density of inclusion,  $\text{kg}/\text{m}^3$ ;  $V$  is the volume of inclusion,  $\text{m}^3$ ; and  $R$  is the radius of inclusion, m.

According to kinetics theory, the mass transfer rate through the concentration boundary is given by:

$$J = Ak\Delta C = 4\pi R^2 k\Delta C \tag{2}$$

where  $J$  is the mass transfer rate, kg/s;  $A$  is the area of mass transfer boundary,  $m^2$ ;  $k$  is the mass transfer coefficient, m/s; and  $\Delta C$  is the difference of concentration,  $kg/m^3$ .

According to the mass conservation law,

$$\frac{dM_p}{dt} = -J \tag{3}$$

That is,

$$\frac{dR}{dt} = -\frac{k\Delta C}{\rho_p} \tag{4}$$

where  $t$  is time, s;  $k$  is related to the flow condition of around fluid, and based on  $Pe$ ,

$$Pe = \frac{2R|u|}{D} \tag{5}$$

$$k = \begin{cases} D/R & Pe \leq 10 \\ \frac{D(4 + 1.21Pe^{2/3})^{1/2}}{2R} & 10 < Pe \leq 10,000 \\ \frac{1.1DPe^{1/3}}{2R} & Pe > 10,000 \end{cases} \tag{6}$$

where  $u$  is the velocity of inclusion, m/s;  $D$  is the diffusion coefficient related to temperature and compositions,  $m^2/s$ ; and  $Pe$  is dimensionless Peclet number and it is the ratio of the advective transport rate and the diffusive transport rate [16].

### 2.4 Coupling method

The motion and dissolution models of inclusions are dynamically coupled, which means that the data are real-time two-way transferred. When the inclusion is totally immersed in slag, the dissolution proceeds at the full speed since the contact area is the largest, but when the inclusion is passing the interface with partly immersed body, here we make an assumption that not only the immersed part has size decline, but also the whole sphere decreases in size uniformly. This is an ideal assumption to simplify the

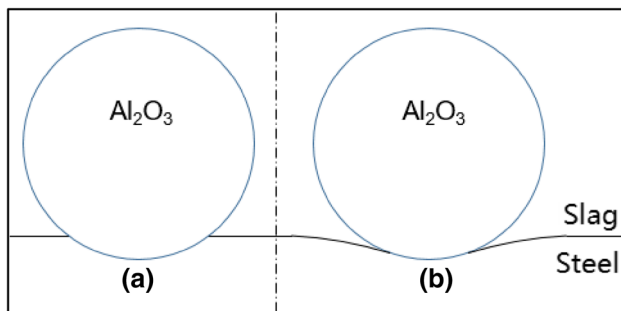


Fig. 1 Schematic diagram of inclusion falling back to interface from slag in motion model (a) and in dissolution model (b)

model, and in reality, the rotation of inclusion may happen and keeps the inclusion a uniform sphere. A coefficient of dissolution,  $Di(Z)$ , is introduced during the transport process to describe the partly immersed condition of dissolution. The dissolution rate is calculated by:

$$\frac{dR}{dt} = -\frac{k\Delta C}{\rho_p} \cdot Di(Z) \tag{7}$$

where  $Di(Z)$  is the ratio of the immersed area in slag to the total inclusion surface area, and it is calculated with Eq. (8)

$$Di(Z^*) = \begin{cases} 0 & Z^* \leq 0 \\ \frac{1}{2} - \frac{\arccos \frac{1-Z^*}{Z^*}}{\pi} & 0 < Z^* \leq 1 \\ \frac{1}{2} + \frac{\arccos \frac{Z^*-1}{Z^*}}{\pi} & 1 < Z^* \leq 2 \\ 1 & Z^* > 2 \end{cases} \tag{8}$$

where  $Z$  is displacement of inclusions, m; and  $Z^*$  is the dimensionless displacement of inclusion,  $Z^* = Z/R$ .

For the inclusion passing the interface and entering the slag, due to its density larger than that of slag, it will fall in slag and come back to the interface. However, its speed is so weak that there will be no chance for it to break the interface again. Thus, for the dissolution process, the inclusion lies above the interface as shown in Fig. 1b, but for the motion model, the force of inclusion is calculated by assuming that the condition is the same as Fig. 1a that the formation of meniscus is neglected.

### 2.5 Parameters

In the IAT motion model, the key properties of three phases are density, viscosity and surface tension. The density and viscosity for the condition studied are given in Table 1.

The interface tension between two phases can be calculated from surface tension. Girifalco and Good [27] built a model of interface tension between phases a and b:

$$\sigma_{ab} = \sigma_a + \sigma_b - \phi_{ab} \sqrt{\sigma_a \cdot \sigma_b} \tag{9}$$

where  $\phi_{ab}$  is the interactive coefficient, which is between 0 – 1 and is obtained from test experiments;  $\sigma_{ab}$  is the interface tension between phase a and phase b, N/m; and  $\sigma_a$  and  $\sigma_b$  are surface tensions of phases a and b, N/m, respectively. The interface tension of inclusion–steel, steel–slag, and inclusion–slag at 1550 °C is 1.518, 1.375, and 0.440 N/m, respectively [11, 24].

The key parameters of the dissolution model are the diffusion coefficient and the concentration difference of alumina. The concentration difference of alumina between the boundary layer and the bulk slag is the driving force of dissolution. The bulk concentration is 17 wt.%, and the

**Table 1** Density and viscosity of alumina, steel and slag at 1550 °C

Property	Density/ (kg m <sup>-3</sup> )	Viscosity/ (Pa s)
Alumina inclusion	3990	+ ∞
Liquid steel	7000	0.0065
Molten slag	2543	0.1998

saturated concentration in the boundary layer at 1600 °C is 49.2 wt.% which is calculated by the thermodynamic database of FactSage<sup>TM</sup> [28].

## 2.6 Initial conditions

The simulation begins just as the inclusion contacts the interface; thus, the initial conditions for the inclusion are its contact size  $R_0$  and velocity  $v$ , and these two parameters determine the initial momentum that the inclusion has. In traditional models, the contact velocity is thought to be Stokes floating terminal velocity, but the  $Re$  number of the inclusion should be under 1 to use this. It was reported that for large-size inclusion, the  $Re$  number is larger than 1 [11, 24], and a model with expanded  $Re$  range is introduced. The comparison of terminal velocity of inclusion with three different sizes in steel with Stokes model and other model is given in Table 2.

Table 2 shows that the velocity calculated by two models is the same for 10- $\mu\text{m}$  inclusion size, but about 10% difference appears for 100- $\mu\text{m}$ - and 1000- $\mu\text{m}$ -diameter inclusions, and the difference is one magnitude. This calculation difference is because the new model considers the drag force with different equations for different  $Re$  ranges, and this comprehensive consideration makes the model more accurate.

## 3 Results and discussion

### 3.1 Motion of inclusion at interface

The competition between the initial momentum of inclusions when it contacts the interface and the resistance decides whether it will break the interface or not. The critical conditions are the size and contact velocity and if

there is no other external force, the contact velocity is the floating terminal velocity, which is only related to the size. Thus, the critical condition is the inclusion size. The motion of three different-size inclusions is shown in Fig. 2.

In Fig. 2, three kinds of moving patterns of inclusion are shown. Pattern (a) shows that small-size inclusion speeds down all the way during the contact with interface and finally stops at the interface. Pattern (b) shows that 100- $\mu\text{m}$  inclusion can march further than the 10- $\mu\text{m}$  inclusion and almost breaks the interface, but at last it is bounced back by the interface and contacts the interface again with smaller velocity and finally is stopped by the interface. Pattern (c) shows that inclusion passes the interface and continues moving in the slag, but due to its larger density than that of the slag, it falls back to the interface and after a few fluctuations, it keeps static above the interface, and only inclusions with this kind of moving pattern can dissolve in the slag phase. The time from the start to the final stop at the interface is different for 10-, 100- and 500- $\mu\text{m}$  size inclusion, which is about 10  $\mu\text{s}$ , 1000  $\mu\text{s}$  and 0.1 s, respectively. The time of contacting the interface is short, even for the large-size inclusions.

### 3.2 Dissolution of inclusion

The dissolution of inclusions starts when it contacts the slag. According to the kinetics theory, the motion of inclusions is in favor of its dissolution, which keeps the concentration around the inclusion renewed continuously. The comparison of dissolution between the static dissolution and moving with terminal velocity in the slag is shown in Fig. 3. It is obvious that motion speeds up the dissolution. However, the time of motion is quite short. Thus, the size change during motion remains unclear. In this study, for the condition simulated, there is no obvious dissolution, and the maximum change in radius is below 1%. This is because the time for dissolution is really short, and most of the dissolution happens when the inclusion lies above the interface with no velocity. The dissolution curve of different-size inclusion is shown in Fig. 4. It can be seen that even though the total time of dissolution varies a lot, the routine or mode of dissolution is the same. The radius of inclusion changes slowly at first but sharply near the end. The relationship between dissolution time and inclusion radius is calculated by the model and shown in Fig. 5.

**Table 2** Floating terminal velocity of different-size inclusion in steel

Diameter/ $\mu\text{m}$	10	100	1000
Stokes floating terminal velocity/(m s <sup>-1</sup> )	$1.19 \times 10^{-4}$	$1.19 \times 10^{-2}$	1.19
Floating terminal velocity according to Refs. [11, 24]/(m s <sup>-1</sup> )	$1.19 \times 10^{-4}$	$9.38 \times 10^{-3}$	0.131

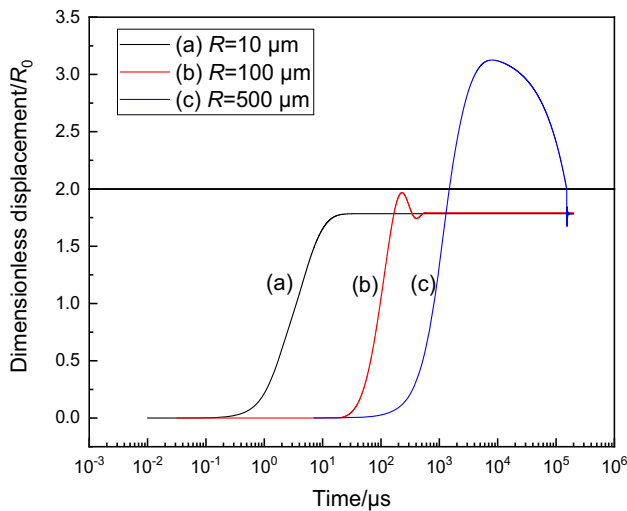


**Fig. 2** Dimensionless displacement of inclusion changes with time. **a** Blocked by interface of small-size inclusion; **b** bounced back by interface of medium-size inclusion; **c** passing interface and entering slag of large-size inclusion

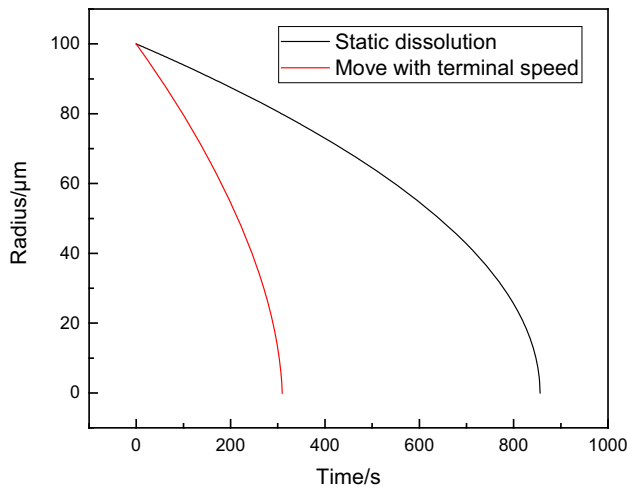


**Fig. 3** Dissolution of 100- $\mu\text{m}$  inclusion in slag with and without motion

### 3.3 Evaluation of dissolution time

Even though the dissolution rate during moving is larger than that in the static condition, the dissolution time is longer for the static removal of inclusion. Thus, the time of different stages of inclusions should be evaluated. The whole process is divided into three stages. Stage I starts when the inclusion contacts the interface and ends when its displacement is  $2R$ . During Stage I, the motion is with a high speed, but the inclusion is just partly contacting the slag; thus, the dissolution rate should be mild. Stage II comes just after Stage I and ends when the inclusion is totally motionless. Stage II has the same high speed to Stage I, but a full contact with slag, and the dissolution

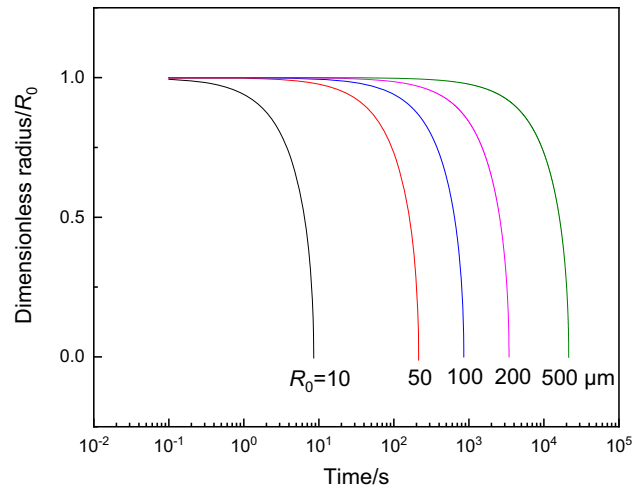


**Fig. 4** Dimensionless radius of inclusion in slag changes with time

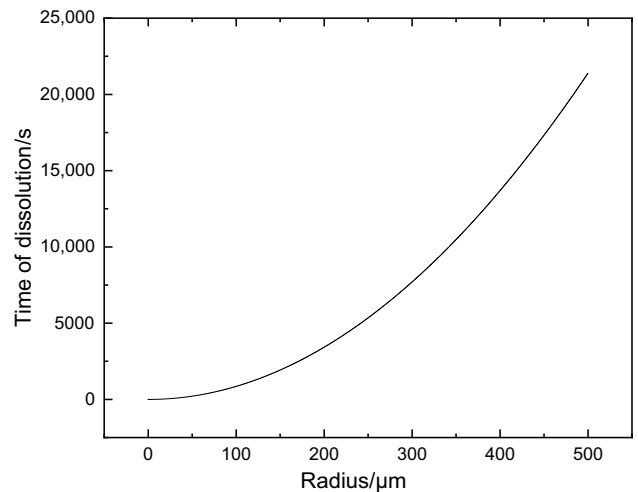


**Fig. 5** Relationship between inclusion radius and time of dissolution

should be the highest. Stage III is the static dissolution time, which follows Stage II and ends when the inclusion totally disappears. The last stage is with the lowest dissolution rate. The time of three stages of different-size inclusion is shown in Fig. 6. Time of Stage I and III changes with inclusion size more apparently than that of Stage II. Probably, this is because large-size inclusion enters slag phase with more momentum, which means that they rise faster in the slag at first. However, the large inclusion falls with large resistance (drag force) and is slower than the smaller one. Thus, the total time of Stage II does not show obvious variation in size. Figure 6 also indicates that three stages are at different time magnitudes, in which Stage I is the shortest and it is seven magnitudes smaller than the longest stage. The time of different stages varies a lot, and Stage III takes more than 99.99% of the total removal time for most inclusions. Therefore, even with the relatively high dissolution rate, the time of the first

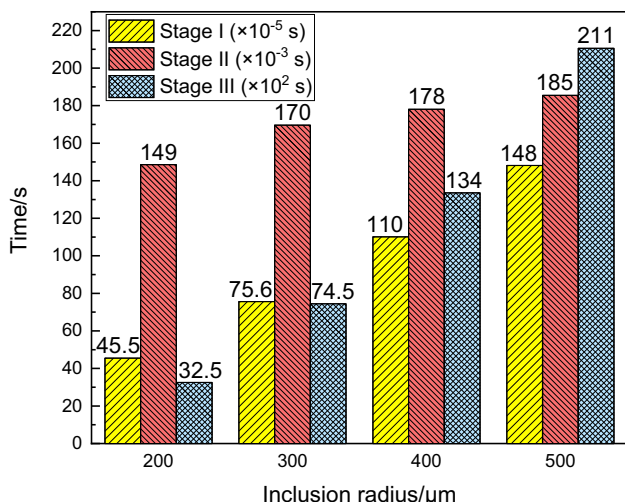


Fig. 6 Time of three stages of different-size inclusions

two stages is too short to show obvious dissolution of inclusions. In fact, during Stage I and II, the total radius change is 0.8 and 2.5% for 200 and 500  $\mu\text{m}$ , respectively, which is negligible compared to the whole dissolution process.

An interesting trend can be seen in Fig. 7 that when the size decreases, the time percentage of the non-static stages (I and II) increases. If the inclusion is small enough, there is a chance that the inclusion moving at interface process will control the dissolution process. However, in this study, an assumption is made that small inclusion which cannot overcome the interface resistance cannot enter the slag phase (For the simulated condition in this study, the critical

radius is 118.23  $\mu\text{m}$ .), and the blocked inclusion will stay just under the interface at the steel side, whereas the IAT motion model just considers the aspect of force balance, and in fact, the wetting process of inclusions with slag is complex. A small alumina inclusion, which cannot enter slag phase immediately after its arriving at interface, may be brought into slag by wetting with slag, interface fluctuation, interaction between inclusions or interaction between inclusions and gas bubble. Sridhar et al. [29–32] tried to in situ observe the separation of inclusions at the interface and found that inclusions with size smaller than critical value stay at the slag side of the interface. However, it is unclear whether the inclusion is just separated from steel or from bigger size one which has dissolved in the slag for a while. Thus, the large-size inclusion will go straightly into the slag phase, and the static dissolution in slag is the controlling step for removing, while the key step for removing the small-size inclusion may be the interaction with interface, which needs further study. For the removal of inclusion, a schematic diagram that illustrates the size and time scale of inclusion during the removal process is shown in Fig. 8.

### 4 Conclusion

A coupled model of the IAT motion model and inclusion dissolution is built to study the controlling step of inclusion removal. The IAT model simulation gives the critical conditions of whether inclusion can enter the slag and start

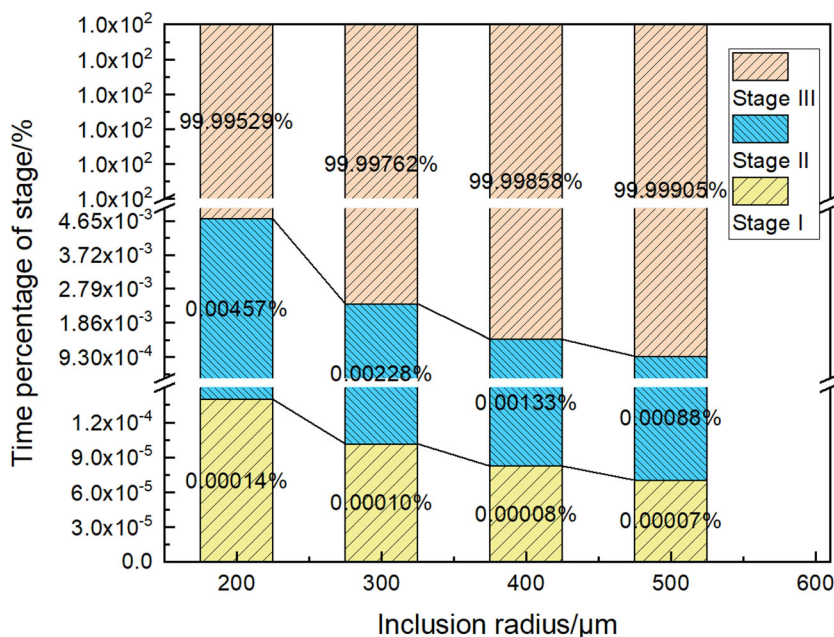
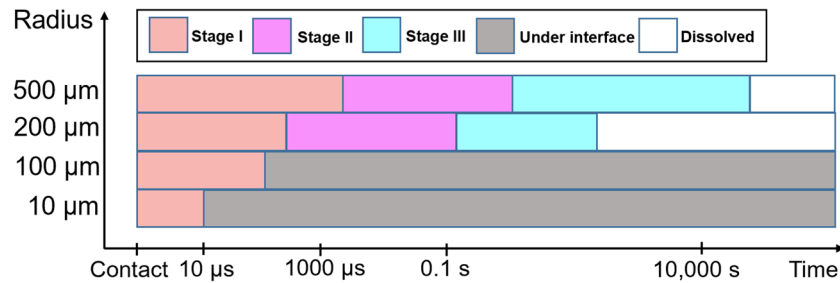


Fig. 7 Time percentage of different stages of different-size inclusions



**Fig. 8** Different stages of inclusion removal with different-size scale

dissolution, which is important to study the inclusion removal.

For the large-size inclusion, the results of this coupled model indicate that the interaction time of inclusions with the interface is negligible compared to the static dissolution time. The dissolution rate of Stage I and II is high due to inclusion motion, but the process is limited by the very short time. Most of the inclusion dissolution occurs at Stage III. For the small-size inclusion, it cannot enter the slag phase straightly when it arrives at the interface according to the IAT model. It is the interaction with interface that limits its removal. However, how the inclusion interacts with interface, whether it will enter slag, and how long it will take need further study.

**Acknowledgments** The authors gratefully acknowledge the support from the National Natural Science Foundation of China (Nos. 51574020 and 51674023).

**Author contributions** Wei Liu and Shu-feng Yang wrote the main manuscript text, and Hong-bo Yang built part of the model.

## References

- [1] H.V. Atkinson, G. Shi, *Prog. Mater. Sci.* 48 (2003) 457–520.
- [2] Y. He, Q. Li, W. Liu, *Metall. Mater. Trans. B* 43 (2012) 1149–1155.
- [3] Z.C. Zhao, R.S. Qin, *Metal. Mater. Trans. B* 48 (2017) 2781–2787.
- [4] K. Takahashi, S. Taniguchi, *ISIJ Int.* 43 (2003) 820–827.
- [5] C. Li, J. Gao, Z. Wang, Z. Guo, *Metall. Mater. Trans. B* 48 (2017) 900–907.
- [6] W. Lou, M. Zhu, *Metall. Mater. Trans. B* 44 (2013) 762–782.
- [7] D.Y. Sheng, M. Söder, P. Jönsson, L. Jonsson, *Scand. J. Metall.* 31 (2002) 134–147.
- [8] L.F. Guo, Y. Wang, H. Li, H.T. Ling, *J. Iron Steel Res. Int.* 20 (2013) No. 7, 35–39.
- [9] Y. Miki, B.G. Thomas, *Metall. Mater. Trans. B* 30 (1999) 639–654.
- [10] L. Zhang, S. Taniguchi, K. Cai, *Metall. Mater. Trans. B* 31 (2000) 253–266.
- [11] S. Yang, W. Liu, J. Li, *JOM* 67 (2015) 2993–3001.
- [12] S. Kimura, Y. Nabeshima, K. Nakajima, S. Mizoguchi, *Metall. Mater. Trans. B* 31 (2000) 1013–1021.
- [13] J. Liu, M. Guo, P.T. Jones, F. Verhaeghe, B. Blanpain, P. Wollants, *J. Eur. Ceram. Soc.* 27 (2007) 1961–1972.
- [14] J.P. Bellot, V. Descotes, A. Jardy, *JOM* 65 (2013) 1164–1172.
- [15] L. Zhang, *JOM* 65 (2013) 1138–1144.
- [16] P. Yan, B.A. Webler, P.C. Pistorius, R.J. Fruehan, *Metall. Mater. Trans. B* 46 (2015) 2414–2418.
- [17] J.H. Park, J.G. Park, D.J. Min, Y.E. Lee, Y.B. Kang, *J. Eur. Ceram. Soc.* 30 (2010) 3181–3186.
- [18] J.H. Park, I.H. Jung, H.G. Lee, *ISIJ Int.* 46 (2006) 1626–1634.
- [19] B.J. Monaghan, L. Chen, *J. Non-Cryst. Solids* 347 (2004) 254–261.
- [20] S.H. Lee, C. Tse, K.W. Yi, P. Misra, V. Chevrier, C. Orrling, S. Sridhar, A.W. Cramb, *J. Non-Cryst. Solids* 282 (2001) 41–48.
- [21] K. Nakajima, K. Okamura, in: *Proc. 4th Int. Conf. on Molten Slags and Fluxes, ISIJ, Sendai, 1992*, pp. 505–510.
- [22] J. Strandh, K. Nakajima, R. Eriksson, P. Jönsson, *ISIJ Int.* 45 (2005) 1597–1606.
- [23] J. Strandh, K. Nakajima, R. Eriksson, P. Jönsson, *ISIJ Int.* 45 (2005) 1838–1847.
- [24] C. Liu, S. Yang, J. Li, L. Zhu, X. Li, *Metall. Mater. Trans. B* 47 (2016) 1882–1892.
- [25] S. Yang, J. Li, C. Liu, L. Sun, H. Yang, *Metall. Mater. Trans. B* 45 (2014) 2453–2463.
- [26] G.N. Shannon, S. Sridhar, *High Temp. Mat. Pr.-Isr.* 24 (2005) 111–124.
- [27] L.A. Girifalco, R.J. Good, *J. Phys. Chem.* 61 (1957) 904–909.
- [28] C.W. Bale, P. Chartrand, S.A. Degterov, G. Eriksson, K. Hack, R.B. Mahfoud, J. Melançon, A.D. Pelton, S. Petersen, *Calphad* 26 (2002) 189–228.
- [29] S. Vantilt, B. Coletti, B. Blanpain, J. Fransaer, P. Wollants, S. Sridhar, *ISIJ Int.* 44 (2004) 1–10.
- [30] B. Coletti, B. Blanpain, S. Vantilt, S. Sridhar, *Metall. Mater. Trans. B* 34 (2003) 533–538.
- [31] P. Misra, S. Sridhar, A.W. Cramb, *Metall. Mater. Trans. B* 32 (2001) 963–967.
- [32] P. Misra, V. Chevrier, S. Sridhar, A.W. Cramb, *Metall. Mater. Trans. B* 31 (2000) 1135–1139.